energies

Article

The Modified Heat Flux Modeling in Nanoparticles (Fe_3O_4 and Aggregation Nanoparticle) Based Fluid between Two Rotating Disks

Hussan Zeb [1], Hafiz Abdul Wahab [1,*], Umar Khan [1] and Mohamed Ehab [2] and Muhammad Yousaf Malik [3]

[1] Department of Mathematics & Statistics, Hazara University, Mansehra 21120, Pakistan; hussan_maths@hu.edu.pk (H.Z.); umar_jadoon@hu.edu.pk (U.K.)
[2] Engineering Mathematics and Physics Department, Faculty of Engineering and Technology, Future University in Egypt, New Cairo 11835, Egypt; mehab@fue.edu.eg
[3] Department of Mathematics, College of Sciences, King Khalid University Abha, Abha 61413, Saudi Arabia; drmymalik@hotmail.com
* Correspondence: wahab@hu.edu.pk

Abstract: In this article, Cattaneo Christov heat transfer analysis in nanofluid (Ferro Fe_3O_4 and Aggregation) flow between two parallel rotating disks with different velocities determined. The relaxation time, velocity slip, heat convective boundary condition, and heat generation are also presented. The governing partial differential equation (PDEs) model is converted into a set of nonlinear ordinary differential equations (ODEs) system by similarity variables. The solution is computed of the resulting ODEs system by using the Runge Kutta (Rk) method. Here a decline is noticed in the tangential velocity for nanoparticles (Fe_3O_4 and Aggregation nanoparticle) for higher values of the porosity parameter (λ_1), slip parameter γ_1, magnetic parameter (M) and Reynolds number (Re_r), while tangential velocity arises for higher values of rotation parameters ($ß_1$). This reduces the temperature field for nanoparticles by higher values of Eckert number (Ec), Prandtl number (Pr), Reynolds number (Re_r), porosity parameter (λ_1), while increases for arising the values of thermal relaxation parameter λ_2, and for both Biot numbers (B_1, B_2) nanoparticles (Fe_3O_4 and Aggregation nanoparticle). Further we compute the characteristics of physical quantities, namely skin friction and Nusselt number are presented.

Keywords: (Ferro Fe_3O_4 and Aggregation) nanoparticle; slip boundary condition; heat sources; two parallel rotating disks

check for updates

Citation: Zeb, H.; Wahab, H.A.; Khan, U.; Ehab, M.; Malik, M.Y. The Modified Heat Flux Modeling in Nanoparticles (Fe_3O_4 and Aggregation Nanoparticle) Based Fluid between Two Rotating Disks. *Energies* **2022**, *15*, 4088. https://doi.org/10.3390/en15114088

Academic Editors: Wasfi A. Shatanawi and Khalil Ur Rehman

Received: 16 April 2022
Accepted: 13 May 2022
Published: 2 June 2022

1. Introduction

Nowadays, mathematicians and engineers have been motivated to study nanofluids because of their significant importance in modern age applications in science, engineering processes, and biomedical sciences. Nanofluid is a stable colloidal mixture of the base fluid (e.g., kerosene, blood, water, Nanoparticle aggregation oil, glycerin, ethylene glycol, etc.) and nanoparticle (Ag, Fe_3O_4, Cu, Au, Ag, SiO_2, TiO_2, Al_2O_3) of diameter 1–100 nm. Many authors broadly exposed the assumption of nanofluids as a unique homogeneous phase that involves thermophysical properties of nanofluids model of their characteristics was explored by Khanafer et al. [1]. The magnetic force effects on heat transfer in ethylene-glycol nanofluid in a complex enclosure reported by Rostami et al. [2]. Waini et al. [3] explored the effects of thermal radiation in MHD flow of hybrid nanofluid by considering a permeable stretching wedge. Devi et al. [4] also investigated the MHD flow of Cu/Al_2O_3/water hybrid and nanofluids due to stretching surface with suction effects. Hossein The ferrofluid over a vertical plate by the considering of lamina- shaped nanoparticle was explored by Hosseinzadeh et al. [5]. Shoaib et al. [6] presented a 3-D MHD flow of hybrid nanofluids with heat transfer over a moving surface. Hassan et al. [7] presented the characteristic of hybrid-nanofluid Cu–Ag/water flow with convective heat transfer by using an inverted cone. The numerical solution for a stagnation point flow of hybrid nanofluid (CuO–Ag/water) was presented by Dinavand et al. [8]. The stability analysis for the stagnation point flow in heat transfer and hybrid nanofluid due to a shrinking sheet was computed by Anuar et al. [9]. The effects of metallic nanoparticles in MHD flow of micropolar fluid through a vertical artery with a six type-tenosis was presented by Ahmad et al. [10]. Yousafi et al. [11] found out the analytical solution effects of stagnation point on steady 3-D seddle/Nodle flow of hybrid nanofluid under the considering of a moving cylinder.

Rotating disc coating is a phenomenon that is uniform and the thin fluid film is formed via horizontal rotating disc. In the last few years, liquid film flow exploration has achieved a tremendous consideration of investigators for its useful applications in many manufacturing industries, science, medicine, and engineering. The liquid film flow has as well practical uses in fiber and cable undercoats. Besides, elastic layer drawing, fluidization of structures, and continuous shaping are also well-known applications of the liquid film. Initially, the concept of liquid film fluid over a rotating disc was reported by Emslie et al. [12]. Refinement of the governing equitation is analyzed by the equilibrium between the viscous and centrifugal forces. The MHD rotating flows of copper/silver water nanofluids over rotating disks in the existence of drag coefficient with thermal radiation effects were reported by Rout et al. [13]. Ahmad et al. [14] reported the Maxwell nanofluid flow between two stretchable rotating disks in the existence of variable thermal conductivity and axial magnetic field. They applied the Buongiorno nanofluid flow model and highlighted the characteristics of lower and upper disks in both the opposite and same directions. The Cattaneo-Christov heat flux model in flow between the two stretchable rotating disks with pours medium was reported by Hayat et al. [15]. Li et al. [16] explored a three-dimensional time-dependent bio-convection flow between two expanding or contracting rotating disks.

Many anthers studied the aggregation nanoparticle in nanofluids can be seen in Figure 1. The heat transfer analysis of nanofluid (aggregation nanoparticle and titaniam) flow in pip was reported by He et al. [17]. The Marangoni convection effects on aggregation nanoparticles of ethylene glycol-based titanium fluid were reported by Mackolil et al. [18]. The impacts of radioactive and aggregation nanoparticles of a nanofluid were studied by Chen et al. [19]. The aggregation nanoparticle effects in nanofliuid between two rotating disks was investigated by Wang et al. [20]. Wang also studied the characteristics of aggregation nanoparticles and magnetic field in over two rotating cones in Ref. [21].

The convective heat boundary condition is a very interesting topic due to its significant importance in heat transfer phenomena. For example, nuclear plants, gas turbines, thermal energy storage, etc. Referring to various industrial and mechanical processes, convective boundary conditions are more practical, including material drying, in-service cooling processes, etc. The convective boundary condition that affects generalized Hybrid nanofluid over horizontal pours stretching a sheet with thermal radiation effects was explored by Asim et al. [22]. The combined effects of a convective boundary condition and chemical reactive species on viscous fluid over a nonlinear curved stretching surface were demonstrated by Sajjad et al. [23]. Hayat et al. [24] explored the convective heat boundary condition in non-Newtonian fluid over a curved stretching sheet having homogeneous and heterogeneous reactions.

Different kinds of heat sources (such as temperature heat sources and space-dependent heat sources) frequently occur in many engineering applications. They increase the temperature profiles as they provide more energy to the system. The heat sources processes play a significant role in the heat transfer phenomena. Saleem et al. [25] demonstrated the effects of external thermal radiation on the nanofluid transport with a variable heat source. They show the result, the temperature profile via the enhancement of a heat source parameter, and a decrement in the concentration profile. The combined effects of thermal radiation and heat source on a three-dimensional generalized fluid with heat transfer rate was reported by Zia et al. [26]. Some recent works on the heat source effects on nanofluid flows can be seen in [27–31].

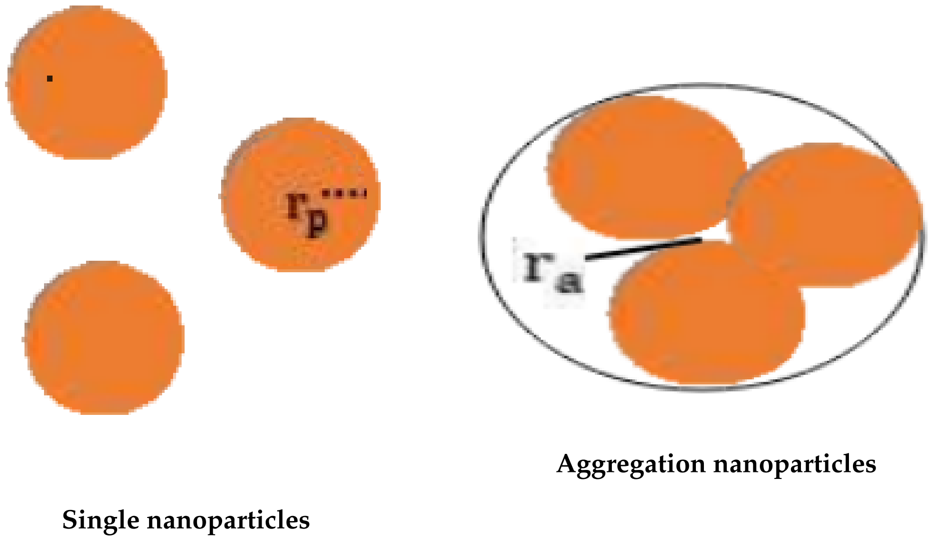

Figure 1. Nanoparticles aggregation where r_a and r_p radii of the aggregated nanoparticles and single nanoparticles respectively.

Inspired from the aforementioned literature review, we have explored the nanofluid (Ferro Fe_3O_4 and aggregation) flow over coaxial rotating disks; however, the convective heat boundary condition has not been investigated yet. The governed PDEs model is transformed into ODEs system by similarity transformation. The solution of the transformed ODEs is computed by the shooting method. The impacts of different physical parameters of the velocity and temperature field have been presented through graphs. Further, we have also presented the effects of different physical parameters of the skin friction and local Nusselt number through the table. The main objectives of the present work are listed as:

- The study of Cattaneo Christov heat flux model in nanofliuid between tow paralla disks.
- The comprehensive study of the nanoliquid flow (with Aggregation and without Aggregation) nanoparticles.
- The characteristics of slip and heat convective boundary conditions are considered.
- The study of heat sources (temperature dependent source and space dependent source) are analyzed.
- To compute the solution of the problem by using the shooting method.

2. Mathematical Formulation

The governing model is presented by assuming the electrically conducting heat flux model in nanofluid (Ferro Fe_3O_4 and Aggregation) flow between two rotating disks in the existence of a magnetic field. Here, pours medium presented between the rotating disks where k_0 represents the permeability constant. The lower disk is placed at $(z = 0)$ whereas the upper disk is placed at distance $z = h$ and can be seen in Figure 2. We intend that a_1 and a_2 denote rotational velocities of the lower and upper disks, respectively and Ω_1 and Ω_2 their respective stretching rate constants. Here we utilize r, ϑ, z cylindrical coordinates and u, v, w are the velocity components. Now the governing model [15,18,32] constructed is as follows

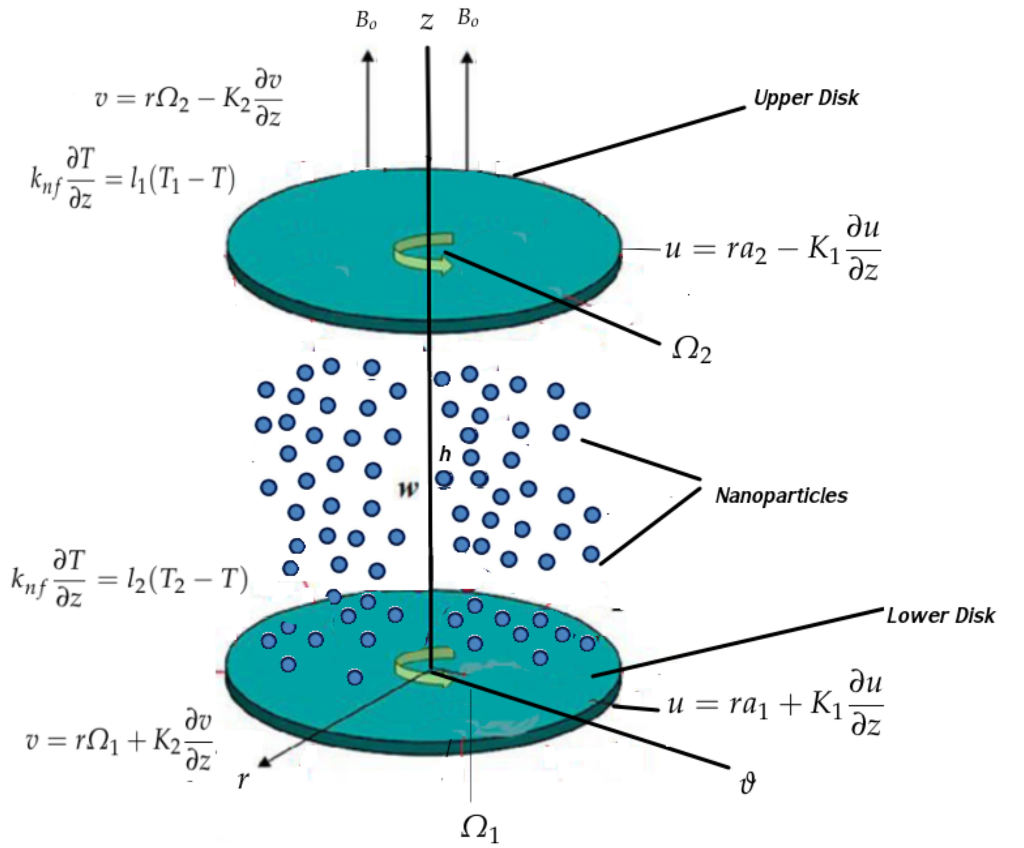

Figure 2. Geometry of the problem.

$$\frac{\partial w}{\partial z} + \frac{\partial u}{\partial r} + \frac{u}{r} = 0 \tag{1}$$

$$\frac{w\partial w}{\partial z} + \frac{u\partial u}{\partial r} - \frac{v^2}{r^2} + \left(-\frac{u}{r^2} + \frac{\partial^2 u}{\partial r^2} + \frac{1}{r}\frac{\partial u}{\partial r} + \frac{\partial^2 u}{\partial z^2}\right)\frac{\mu_{nf}}{\rho_{nf}}\frac{u}{\kappa_o} - \frac{1}{\rho_{nf}}\frac{\partial p}{\partial r} - \frac{\sigma_{nf}}{\rho_{nf}}B^2 u, \tag{2}$$

$$\frac{w\partial v}{\partial z} + \frac{u\partial v}{\partial r} - \frac{vu}{r} = \left(-\frac{v}{r^2} + \frac{\partial^2 v}{\partial r^2} + \frac{1}{r}\frac{\partial v}{\partial r} + \frac{\partial^2 v}{\partial z^2}\right) + \frac{\mu_{nf}}{\rho_{nf}}\frac{v}{\kappa_o} - \frac{1}{\rho_{nf}}\frac{\partial p}{\partial r} - \frac{\sigma_{nf}}{\rho_{nf}}B^2 v, \tag{3}$$

$$\frac{w\partial w}{\partial z} + \frac{u\partial w}{\partial r} = \left(\frac{1}{r}\frac{\partial w}{\partial r} + \frac{\partial^2 w}{\partial r^2} + \frac{\partial^2 w}{\partial z^2} + \frac{\partial^2 w}{\partial u^2}\right) + \frac{\mu_{nf}}{\rho_{nf}}\frac{w}{\kappa_o} - \frac{1}{\rho_{nf}}\frac{\partial p}{\partial z} + \frac{v^2}{r^2}, \tag{4}$$

$$(\rho Cp)_{nf}\left(\frac{w\partial T}{\partial z} + \frac{u\partial T}{\partial r}\right) = \sigma_{nf}B_o^2(u^2 + v^2) + \nabla.q, \tag{5}$$

boundary conditions

$$\begin{aligned} u &= ra_1 + K_1\frac{\partial u}{\partial z}, v = r\Omega_1 + K_2\frac{\partial v}{\partial z}, w = 0, k_{nf}\frac{\partial T}{\partial z} = l_1(T_1 - T) \text{ at } z = 0, \\ u &= ra_2 - K_1\frac{\partial u}{\partial z}, v = r\Omega_2 - K_2\frac{\partial v}{\partial z}, w = 0, k_{nf}\frac{\partial T}{\partial z} = l_2(T_2 - T) \text{ at } z = h, \end{aligned} \tag{6}$$

in the aforementioned calculation p and T are taken for pressure and temperature, T_1 and T_2 represents the temperature at the lower and upper disc, respectively. Let K_1, K_2 be the velocity slip parameter and q is taken for heat flux.

$$q + \Upsilon\left(\frac{\partial q}{\partial t} + V.\nabla.q - q.\nabla V + (\nabla.V)q\right) = 0, \tag{7}$$

here k_{nf} and Υ represent the thermal conductivity of the nanofluid and thermal relaxation. Now we simplify the Equations (5) and (7) it can be expressed as follows

$$\begin{aligned}&\frac{w\partial T}{\partial z}+\frac{u\partial T}{\partial r}=\left(\frac{\partial^2 T}{\partial z^2}+\frac{1}{r}\frac{\partial T}{\partial r}\right)-\Upsilon\left[u^2\frac{\partial^2 T}{\partial r^2}+2wu\frac{\partial^2 T}{\partial r\partial z}+w^2\frac{\partial^2 T}{\partial z^2}+\left(\frac{w\partial u}{\partial z}+\frac{u\partial u}{\partial r}\right)\frac{\partial T}{\partial r}\right.\\&\left.+\left(\frac{w\partial w}{\partial z}+\frac{u\partial w}{\partial r}\right)\frac{\partial T}{\partial z}\right]+\sigma_{nf}B_o 2(u^2+v^2).\end{aligned} \tag{8}$$

Now we utilize the von-Kamran similarity transformations to transform the governing PDEs into nonlinear coupled ODEs

$$\begin{aligned}&u=r\Omega_1 f'(\xi), v=r\Omega_1 g'(\xi), w=-2h\Omega_1 f(\xi), \theta=\frac{T-T_2}{T_1-T_2},\\&p=\rho_{nf}\Omega_1\nu_{nf}(p\xi+0.5\frac{\varepsilon r^2}{h}), \xi=\frac{z}{h}.\end{aligned} \tag{9}$$

The law conservation of mass identically satisfied, the Equations (1)–(9) and using Tables 1 and 2 can be expressed as follows

$$\begin{aligned}&f'''-\frac{A_1}{A_2}\zeta+A_1 Re_r\left(-\frac{A_2 M f'}{A_5}-f'^2-\frac{f'}{\lambda_1}+2ff''+g^2\right)=0,\\&2A_1 Re_r\left(-\frac{A_2 M g}{A_5}+\frac{1}{2\lambda_1}g+fg'-fg\right)+g''=0,\\&P'-\frac{2Re_r A_2 f}{BA_1}+2\frac{A_1}{A_2}f''-4Re_r A_2 ff'=0,\\&\frac{A_4\theta''}{Pr}-4A_3\lambda_2 Re_r\left(f^2\theta''+f\theta' f'\right)+2A_3 Re_r f\theta'-EcMA_5 Re_r\left(f'^2+g^2\right)=0,\end{aligned} \tag{10}$$

the boundary conditions

$$\begin{aligned}&f(0)=0, f'(0)=ß_1+\gamma_1 f''(0), \theta'(0)+\frac{B_1(1-\theta(0)}{A_4}=0,\\&g(0)=1+\gamma_2 g'(0), P(0)=0,\\&f(1)=0, f'(1)=ß_2-\gamma_1 f''(1), \theta'(1)+\frac{B_2\theta(1)}{A_4}=0,\\&g(1)=ß_3-\gamma_2 g'(1).\end{aligned} \tag{11}$$

The magnetic parameter, Prandtl number, porosity parameter, Eckert number, thermal relaxation, Velocity slip parameters are listed below $M=\frac{B_o^2\sigma_f o\Omega_1}{\rho_f}$, $ß_2=\frac{\Omega_2}{\Omega_1}$,$Pr=\frac{\mu C_p}{k_1}$, $ß_3=\frac{\Omega_1}{\Omega_1}$, $\lambda_1=\frac{k_o\Omega_1}{rho_{nf}}$ $Ec=\frac{r^2\Omega_1}{Cp(T_1-T_2)}$,$\lambda_1=\Omega_1\gamma$ and $\gamma_1=\frac{K_1}{h}$ and $\gamma_2=\frac{K_2}{h}$,$ß_1$, $ß_2$ and $ß_3$ be the rotation parameters, B_1 and B_2 is the Biot numbers.

Table 1. Thermophysical aspects of different fluid and nanofluid can be seen in Ref. [22].

Properties	H_2O Water	Fe_3O_4 Ferro
ρ (kgm^{-3})	997.1	5180
Cp (JK^{-1}/kg)	4180.0	650
k ($W\ m^{-1}/K$)	0.6071	9.7
σ (s/m)	0.05	0.74×10^7

Table 2. Thermophysical aspects of different fluid and nanofluid.

Properties	Without Aggregation	With Aggregation
Dynamic viscosity	$\frac{\mu_{nf}}{\mu_f} = A_1 = (1-\phi)^{2.5};$	$\frac{\mu_{nf}}{\mu_f} = C_1 = \left(1 - \frac{\phi_a}{\phi_m}\right)^{\xi\phi_m}$
Density	$\frac{\rho_{nf}}{\rho_f} = A_2 = \frac{\phi\rho_s}{\rho_f} + (1-\phi)$	$\frac{\rho_{nf}}{\rho_f} = C_2 = \frac{\phi_a\rho_s}{\rho_f} + (1-\phi_a)$
Specific heat capacity	$\frac{(\rho Cp)_{nf}}{(\rho Cp)_f} = A_3 = \frac{\phi\rho Cp_s}{\rho Cp_f} - \phi + 1$	$\frac{(\rho cp)_{nf}}{(\rho Cp)_f} = C_3 = \frac{\phi_a\rho Cp_s}{\rho Cp_f} - \phi_a + 1$
Thermal conductivity	$\frac{K_{nf}}{k_f} = A_4 = \frac{(2k_f+k_s)-2\phi(k_f-k_s)}{\phi(k_f-k_s)+(2k_f+k_s)}$	$\frac{K_{nf}}{k_f} = C_4 = \frac{(k_a+2k_f)-2\phi_a(k_f-k_a)}{\phi_a(k_f-k_a)+(k_a+2k_f)};$
Electrical conductivity	$\frac{\sigma e_{nf}}{\sigma e_f} = A_5 = \frac{3\phi\left(\frac{\sigma_s}{\sigma_f}-1\right)}{\left(\frac{\sigma_s}{\sigma_f}+2\right)-\phi\left(\frac{\sigma_s}{\sigma_f}-1\right)} + 1$	$\frac{\sigma e_{nf}}{\sigma e_f} = C_5 = \frac{3\phi_a\left(\frac{\sigma_s}{\sigma_f}-1\right)}{\left(\frac{\sigma_s}{\sigma_f}+2\right)-\phi_a\left(\frac{\sigma_s}{\sigma_f}-1\right)} + 1$

The experimental analysis of the EG-based titanium was presented by Chen et al. [19]. The ϕ_a represent the aggregate volume fraction over the largest volume fraction and it is given by $\phi_a = \phi\left(\frac{r_a}{r_p}\right)^{-D+3}$, where $D = 1.8$, $\frac{r_a}{r_p} = 3.34$ and $\eta_a = 2.5$ represent the spherical aggregates and diffusion-limited aggregation, which are the experimental values of the EG-titanium nanoparticle seen in [19]. The thermal conductivity in the aggregation model of Maxwell fluid is expressed as

$$k_a = \frac{1}{4}k_f\left(\frac{(3\phi_{\text{in}}-1)k_s}{k_f} + \left(\left(\frac{(3\phi_{\text{in}}-1)k_s}{k_f} + (3(1-\phi_{\text{in}})-1)\right)^2 + \frac{8k_s}{k_f}\right)^{0.5} + (3(1-\phi_{\text{in}})-1)\right) \tag{12}$$

where $\phi_{in} = (\frac{r_a}{r_p})^{-D+3}$. Differentiating Equation (10)

$$f'''' + A_1 Re_r\left(-\frac{A_2 M f''}{A_5} - f''^2 - \frac{f''}{\lambda_1} + 2ff''' + 2gg'\right) = 0, \tag{13}$$

the pressure gradient ζ in Equation (10) is

$$\zeta = A_1 Re_r\left(-\frac{A_2 M f''(0)}{A_5} + \frac{f'(0)}{\lambda_1} + 2f(0)f'^2(0) - g'(0)^2 + f\right) + f'''(0)\frac{A_1}{A_2}, \tag{14}$$

now integrating the Equation (14) we have

$$P = \frac{2A_2}{A_1}f' + \frac{2Re_r 2A_2}{A_1}\int_0^{\xi} f d\xi + \frac{2A_2}{A_1}f'(0) - 2Re_r f^2 \tag{15}$$

3. Physical Quantities

3.1. Skin Friction

The skin friction coefficient at the lower (Cf_1) disc and upper Cf_2 disc are formulated as

$$Cf_1 = \frac{\tau_w|_{z=0}}{\rho_f(r\Omega_1)^2}, \quad Cf_2 = \frac{\tau_w|_{z=h}}{\rho_f(r\Omega_2)^2}, \tag{16}$$

here τ_w represents the total shear stress and it is formulated as

$$\tau_w = (\tau_{rz}^2 + \tau_{z\theta}^2)^{\frac{1}{2}}, \tag{17}$$

the shear stress τ_{rz} and the tangential stress $\tau_{\theta z}$ are expressed as

$$\begin{aligned} \tau_{rz} &= \mu_{nf} u_z|_{z=0} = \mu_f \frac{r\Omega_1 f''(0)}{hA_1}, \\ \tau_{\theta z} &= \mu_{nf} u_z|_{z=0} = \mu_f \frac{r\Omega_1 g'(0)}{hA_1}, \end{aligned} \tag{18}$$

the total shear stress arrives at

$$\begin{aligned} Cf_1 Re_r &= \frac{\sqrt{f''(0)^2 + g'(0)^2}}{(1-\phi)^2.5}, \\ Cf_2 Re_r &= \frac{\sqrt{f''(1)^2 + g'(1)^2}}{(1-\phi)^2.5}. \end{aligned} \tag{19}$$

3.2. Nusselt Number

The Nusselt number (Nu_{xa} and Nu_{xb}) at the lower and upper discs are defined as

$$\begin{aligned} Nu_{x1} &= \frac{hq_w}{k_f(T_1 - T_2)}\bigg|_{z=0}, \\ Nu_{x2} &= \frac{hq_w}{k_f(T_1 - T_2)}\bigg|_{z=h}, \end{aligned} \tag{20}$$

where q_w stands for heat flux at the rotating disc, it can be formulated as

$$\begin{aligned} q_w &= -k_{nf} = \frac{\partial T}{\partial z}|_{z=0} = -(T_1 - T_2)k_{nf}\theta'(0), \\ q_w &= -k_{nf} = \frac{\partial T}{\partial z}|_{z=h} = -(T_1 - T_2)k_{nf}\theta'(1). \end{aligned} \tag{21}$$

the dimensionless form can be displayed as

$$\begin{aligned} Nu_{xa} &= -A_4\theta(0), \\ Nu_{xb} &= -A_4\theta'(1). \end{aligned} \tag{22}$$

4. Shooting Method

A shooting method is a numerical approach, generally used for the solution of the BVP by reducing it to the system of an initial value problem. Further detail can be seen in the book (Ref. [33], Chapter 8). The Equations (10) and (13) are the system of non-linear coupled ODEs of order four in $f(\xi)$, order two in $g(\zeta)$ and order two in $\theta(\zeta)$, respectively. The rearranging of the Equations (10) and (13) with boundary conditions will take the form

$$\begin{aligned} f'''' &= -A_1 Re_r\left(-\frac{A_2 M f''}{A_5} - f''^2 - \frac{f''}{\lambda_1} + 2ff''' + 2gg'\right), \\ g'' &= -2A_1 Re_r\left(-\frac{A_2 M g}{A_5} + \frac{1}{2\lambda_1}g + fg'\right) \\ \theta'' &= Pr Re_r \frac{4A_3\lambda_2(f\theta' f') - 2A_3 f\theta' - EcMA_5(f'^2 + g^2)}{A_4 - 4A_3 Re_r f^2}. \end{aligned} \tag{23}$$

To reduce the higher order nonlinear coupled ODEs into a first order ODEs system, let us consider

$$\begin{aligned} &g = u_1,\ g' = u_2,\ \ g'' = u_3 \text{ and } u_3' = u_3', \\ &\theta = u_4,\ \ \theta' = u_5 \ \text{ and } \ \theta'' = u_5', \end{aligned} \tag{24}$$

the nonlinear coupled ODEs system is reduced into a first order ODEs system; it can be arranged in a new variable, which is given by:

$$\begin{aligned}
u_1' &= u_2,\\
u_2' &= u_3,\\
u_3' &= u_4,\\
u_4' &= A_1 Re_r\left(-\frac{A_2 M u_3}{A_5} - u_3^2 - \frac{u_3}{\lambda_1} + 2u_1u_4 + 2u_5u_6\right),\\
u_5' &= u_6,\\
u_6' &= -2A_1 Re_r\left(u_1u_6 - \frac{A_2 M u_5}{A_5} + \frac{1}{2\lambda_1}u_5 - u_2u_5\right),\\
u_7 &= u_8,\\
u_8' &= Pr Re_r \frac{4A_3\lambda_2(u_1u_2u_8 f') - 2A_3u_1\theta' - EcMA_5\left(u_2^2 + u_5^2\right)}{A_4 - 4A_3 Re_r u_1^2},
\end{aligned} \tag{25}$$

boundary conditions are

$$\begin{aligned}
&u_1(0) = 0, u_2(0) = ß_1 + \gamma_1 u_3(0), \frac{B_1(1 - u_7(0))}{A_4} + u_8(0) = 0, u_5(0) = 1 + \gamma_2 u_6(0),\\
&u_2(1) = ß_2 - \gamma_1 u_3(1)), \frac{u_7(1)B_2}{A_4} + u_8(1) = 0, u_1(1) = 0, u_5(1) = ß_3 - \gamma_2 u_6.
\end{aligned} \tag{26}$$

To solve the above seven order ODEs system Equation (26) via a shooting method with RK-45. Seven initial guesses are required, whereas four initial guesses are given and the other three initial guesses $u_2(\zeta)$, $u_5(\zeta)$, and $u_7(\zeta)$ is defined as $\zeta \to 1$. Hence, it is considered that $(u_2(0), u_5(0), u_7) = (q_1, q_2, q_3)$. These unknown three initial guesses $(u_2(0), u_5, u_7(0))$ are computed by a Newton iterative scheme. The main step of this numerical solution is to select the suitable finite values for boundary conditions. The step size and convergence criteria are taken as $\triangle = 0.02$ and $TOL = 10^{-5}$, respectively, for our numerical solution.

5. Validity of the Numerical Solution

In this section, we validate our numerical results with the previously published work. The comparison of $f''(0)$ and $g'(0)$, shown in Table 3, reveals that we found a good agreement between these two methods. We have to evaluate the accuracy of the current method. For this, we computed the different values of $ß_3$. We used a shooting method programming in MATLAB with step size $h = 0.02$ to obtain the velocities and temperatures profiles.

Table 3. Validation the current solution with previous published data when $\gamma_1 = \gamma_2 = M = \phi = ß_1 = ß = \lambda_1 = 0$ and $Re_r = 1$.

$ß_3$	$f''(0)$			$g'(0)$		
	Hosseinzadeh et al. [34]	**Raju et al. [35]**	**Present Work**	**Hosseinzadeh et al. [34]**	**Raju et al. [35]**	**Present Work**
−0.3	0.1039497753	0.10394927	0.1039494	1.304432381	1.30443757	1.3044354
0.0	0.09996773288	0.09996441	0.0999676	1.004285714	1.00428589	1.0042856
0.5	0.06663026596	0.06663987	0.0666397	0.502619047	0.50261334	0.5026132

6. Results and Discussion

In this section, we have demonstrated the physical importance of involving various physical parameters on velocities (i.e., Axial $f(0)$, radial, $g(0)$ and tangential velocity $f'(0)$) and temperature profiles and taking the values $n = 1.0, \gamma_1 = 0.4, \gamma_2 = 0.4; B_1 = 0.5,$

$\lambda_1 = 0.5$, $ß_3 = 0.8, ß_2 = 0.4, Ec = 0.4, \Pr = 6.2, R = 1.5, M = 0.5, ß_1 = 0.5, \lambda_2 = 1.0$ and $B_2 = 0.4$. Further, we explored the characteristics of different physical parameters on local skin friction and Nusselt number via graph as well as table.

6.1. Radial and Axial Velocities

Impacts of rotating of lower disc $ß_1$ on axial and radial velocities is presented in Figures 3 and 4 for both fluids (Aggregation and without aggregation) based on nanofluid. Reductions in the radial and axial velocities at the lower disc due to the rotation parameter of lower disc arises continuously, and another end of the axial and radial velocities arises for higher values of rotation parameter at the lower disc via the increasing values in $ß_1$. The influence of the rotation parameter $ß_2$ on radial and axial velocities is demonstrated in Figures 5 and 6 for both fluid (Aggregation and without aggregation) based on nanofluid. The decaying velocities at the lower disc are represented in $ß_2$. A profile of arising velocities near the upper disc due to the rotation rate of the upper disc is greater.

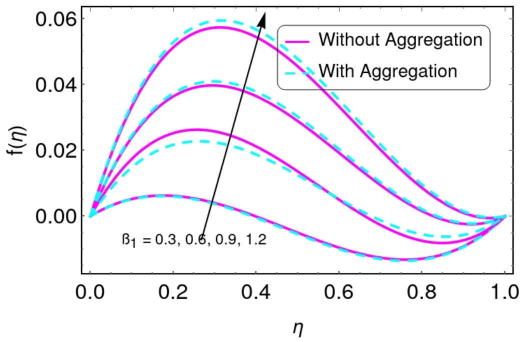

Figure 3. Characteristics of $ß_1$ for $f(\eta)$.

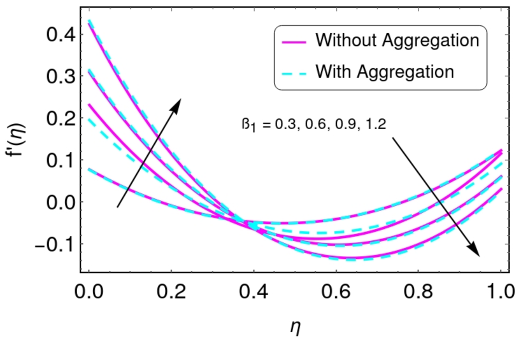

Figure 4. The result of $ß_1$ on $f(\eta)$.

Figures 7 and 8 are for the plot the effects of the velocity slip parameter on axial and radial velocities. This reduces the radial velocity of the fluid near the lower and upper disc by higher values of slip parameter γ_1. The variation of radial velocity rapidly reduces at two points of ξ 0.2 to 0.75. The axial velocity $f(\xi)$ is reduced by greater values of γ_1 therefore, there is less transport of momentum in the radial direction. The characteristics of radial and axial velocities for Reynolds number Re_r is depicted in Figures 9 and 10 for both fluid (Aggregation and without aggregation) based on the nanofluid. The radial and axial velocities reduce at the lower disc for greater values of Re_r. It is fact that the inertial forces have a direct relation with the Reynold number Re_r. The velocity of the upper disc is greater than the lower disc. Due to this fact, there are negative values at the lower disk.

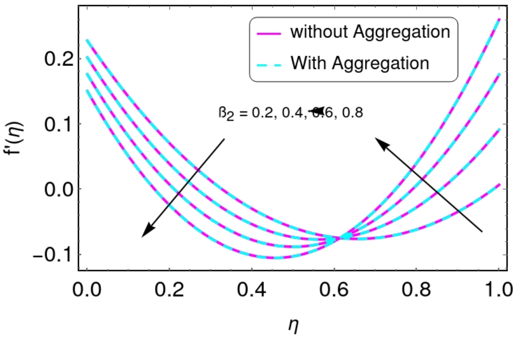

Figure 5. Characteristics of $ß_2$ for f'.

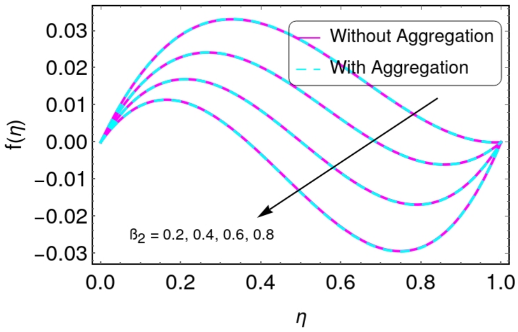

Figure 6. The results of $ß_2$ on $f(\eta)$.

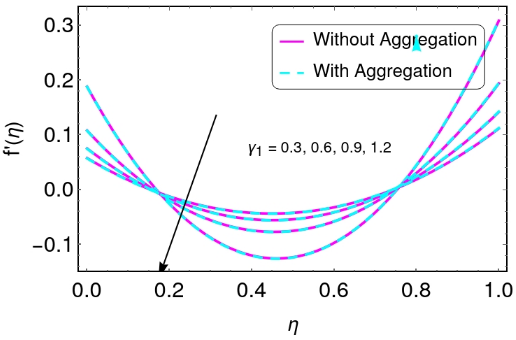

Figure 7. Characteristics of γ_1 for distribution $f'(\eta)$.

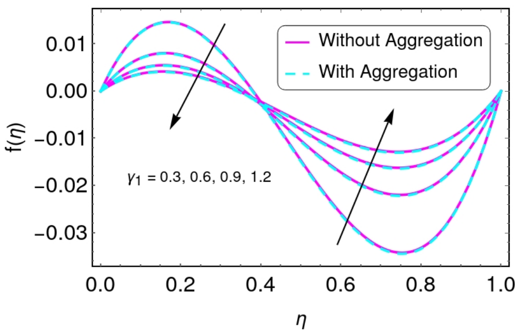

Figure 8. Characteristics of γ_1 for distribution $f(\eta)$.

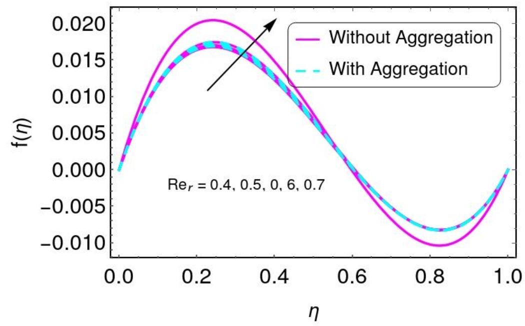

Figure 9. The results of Re_r on $f(\eta)$.

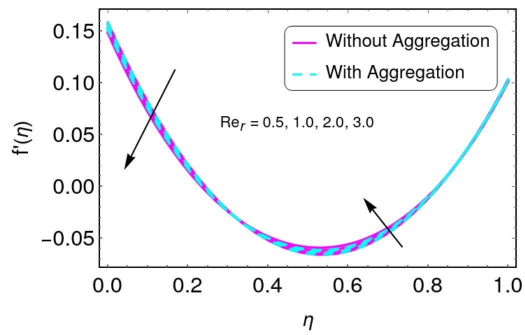

Figure 10. Characteristics of Re_r for $f'(\eta)$.

6.2. Tangential Velocity

Figure 11 represents the impacts of Reynolds number Re_r on tangential velocity for both fluids (Aggregation and without aggregation) based on the nanofluid. Here it is found that the velocity $g(\eta)$ arises by higher values of Re_r for both fluid (Aggregation and without aggregation) based on the nanofluid. The magnitude of tangential velocity for higher values of ß$_3$ is shown in Figure 12. Here it is noticed that the tangential velocity by the higher values of ß$_3$ arises for both fluids (Aggregation and without aggregation) based on the nanofluid. The tangential velocity behavior is plotted in Figure 13 by different values of λ_1. Decreases in the tangential velocity for both nanoparticles (Fe_3O_4 and Aggregation) are based on the nanofluid by the larger values of λ_1. It is concluded from this result, generally, that the porous medium allows the restive flow to arrise due to this fact of the fluid motion being reduced. The effects of the slip parameter on the velocities component demonstrated in Figure 14 for both fluid (Fe_3O_4-and Aggregation) based on the nanofluid. Here it can be concluded that reductions in the velocities components for higher values of slip γ_2 for both (Fe_3O_4 and Aggregation) based on the nanofluid.

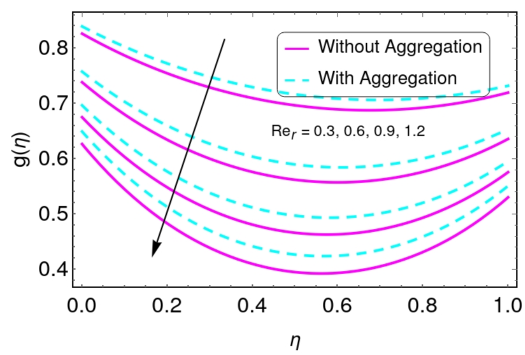

Figure 11. The results of Re_r on $g(\eta)$.

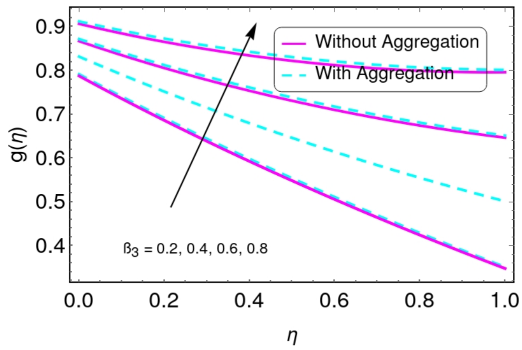

Figure 12. The results of ß$_3$ on $g(\eta)$.

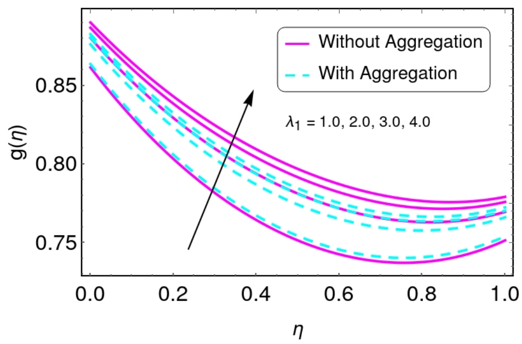

Figure 13. Characteristics of λ_1 for g'.

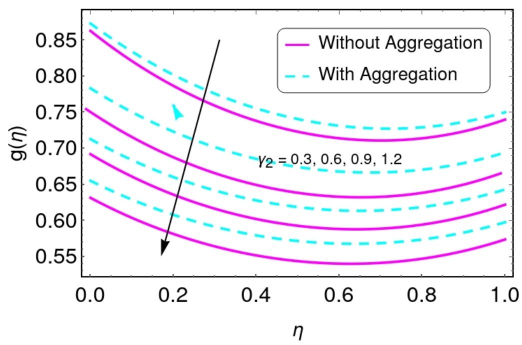

Figure 14. Characteristics of γ_2 for $g(\eta)$.

6.3. Temperature Profile

The temperature field highlighted for greater values of Prandtl number Pr is illustrated in Figure 15. It is noticed that, according to the definition of Prandtl, the higher Prandtl number means the thermal diffusivity becomes smaller; therefore, reducing the temperature field for both (Aggregation and without Aggregation) based on the nanofluid. The importance of the Eckert number on the temperature field for both Fe_3O_4 and Aggregation based on the nanofluid is presented in Figure 16. Since the relation between kinetic energy and enthalpy of the given fluid is presented by the Eckert number. This means that heat is stored in the fluid due to the increasing Eckert number Ec.

The reducing of the temperature field by higher values of relaxation time parameter for both (Fe_3O_4 and Aggregation) based on the nanofluid is presented in Figure 17. It is noticed that thermal relaxation time arises for higher values of λ_2. It implies the particles need more time than their neighboring particles, so, the temperature field is reduced.

The tendency of the fluid temperature is plotted in Figure 18 for greater values of Re_r. It is seen from the figure, reductions in the fluid temperature by greater values of Re_r for both Fe_3O_4 and Aggregation based on the nanofluid. Physically, the inertial forces arise for higher values of Re_r. Therefore, the temperature profile is reduced. The magnitude of temperature for both fluid (Aggregation and without Aggregation) based on the nanofluid by higher values of B_1 and B_2 are shown in Figures 19 and 20. It is found, the temperature field reduces for both fluid (Aggregation and without Aggregation) based on the nanofluid by improving values of B_1 and B_2.

Figure 21 presents the impacts of ϕ on tangential velocity of the fluid for both nanofluid (Fe_3O_4 and Aggregation nanoparticle). Here there are reductions in the tangential velocity profile by increasing the values ϕ. This is due to the enhancement of the volume fraction of nanoparticles. Figure 22 presents the impacts of ϕ on temperature of the fluid both nanofluid (Fe_3O_4 and Aggregation nanoparticle). Here, the temperature field increases by increasing the values ϕ. This is due to the enhancement of the volume fraction of nanoparticles.

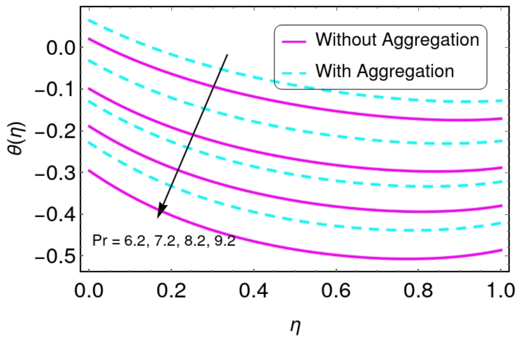

Figure 15. Characteristics of Pr for $\theta(\eta)$.

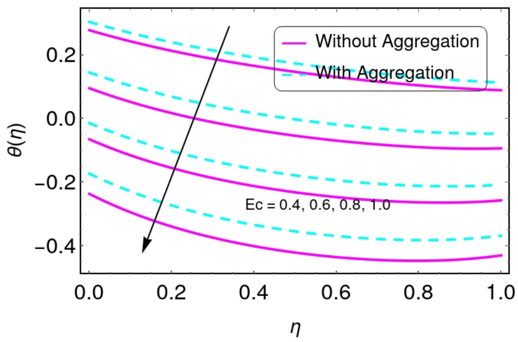

Figure 16. Characteristics of Ec for $\theta(\eta)$.

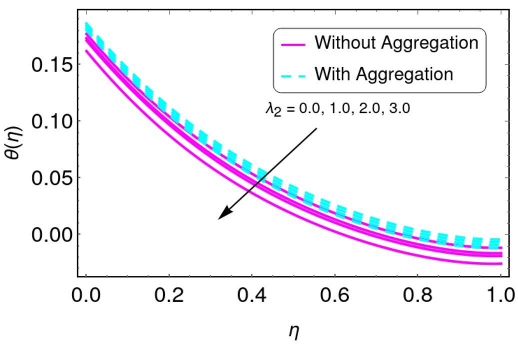

Figure 17. Characteristics of β for $\theta(\eta)$.

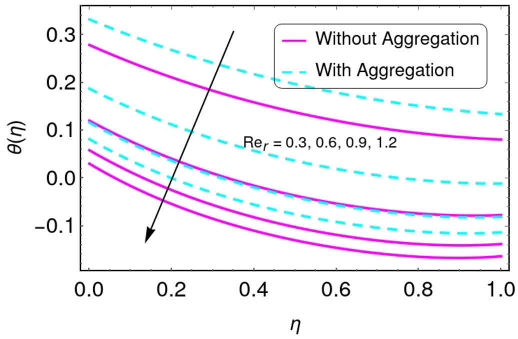

Figure 18. The result of Re_r on $\theta(\eta)$.

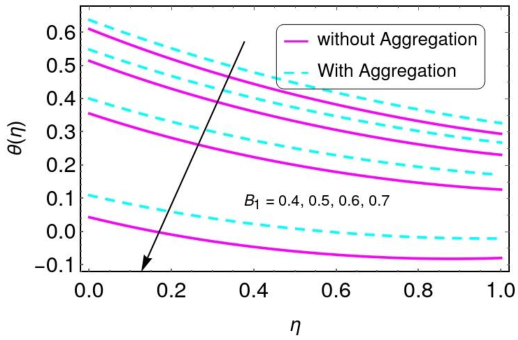

Figure 19. Characteristics of B_1 for $\theta(\eta)$.

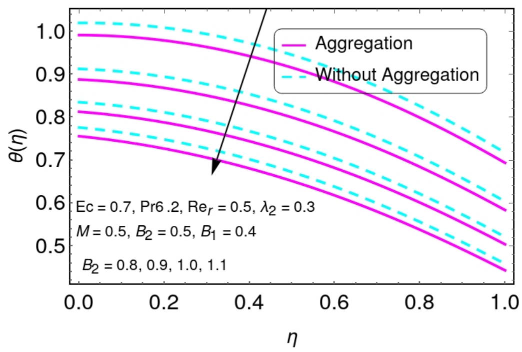

Figure 20. Characteristics of B_2 for $\theta(\eta)$.

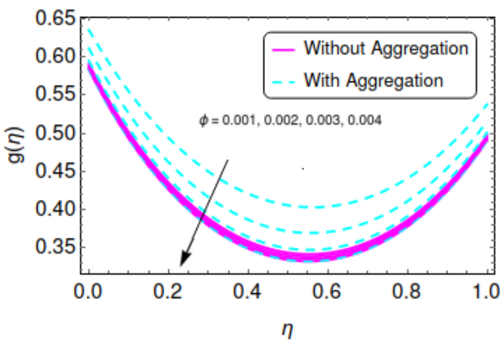

Figure 21. Characteristics of ϕ for $g(\eta)$.

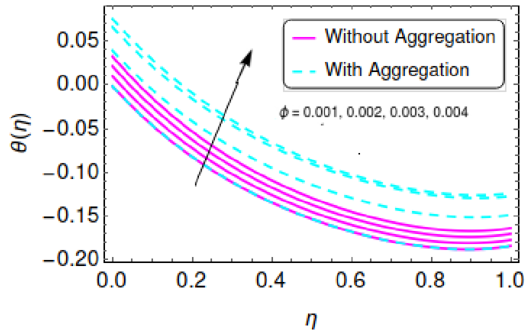

Figure 22. The result of ϕ on $\theta(\eta)$.

The skin friction noticed enhance for higher values of Re_r, ß$_1$, ß$_2$ for both disks while it reduce for by higher λ_1 can be seen in Table 4. It can be observed from Table 5 that the transfer of heat is reduces by greater values of Re_r, Pr, B_1 and λ_2 at both disc.

Table 4. Skin friction for higher vales of Re_r, ß$_1$, ß$_2$ and λ_1.

Re_r	M	ß$_1$	ß$_2$	ß$_3$	λ_1	$C_r a Re_r$ Aggregation	$C_r a Re_r$ Ferro Fe_3O_4	$C_r b Re_r$ Aggregation	$C_r b Re_r$ Aggregation
0.3	1.0	0.5	0.4	0.5	1.0	1.59747	2.67953	3.19359	2.37679
0.6						1.61142	2.84218	3.19359	4.28574
0.9						1.61651	2.98472	3.19359	4.49434
1.2						1.61882	3.10041	3.19359	4.68053
0.3	0.0	0.5	0.4	0.5	1.0	1.52958	2.29524	2.29219	2.29524
	0.5					1.56974	2.34557	2.48519	3.76718
	1.0					1.59747	2.37679	2.67955	4.05128
	1.5					1.61255	2.38949	2.87299	4.31965
0.3	1.0	0.3	0.4	0.5	1.0	1.59747	2.37679	2.67953	2.37679
		0.6				1.59747	2.37679	2.67955	4.05128
		0.9				1.59747	2.37679	2.67955	4.05128
		1.2				1.59747	2.37679	2.67955	4.05128
0.3	1.0	0.5	0.3	0.5	1.0	1.59747	2.37679	2.67953	2.37679
			0.6			1.59747	2.37679	2.67955	4.05128
			0.9			1.59747	2.37679	2.67955	4.05128
			1.2			1.59747	2.37679	2.67955	4.05128
0.3	1.0	0.5	0.4	0.3	1.0	1.59747	2.37679	2.67953	2.37679
				0.6		1.59747	2.37679	2.67955	4.05128
				0.9		1.59747	2.37679	2.67955	4.05128
				1.2		1.59747	2.37679	2.67955	4.05128
0.3	1.0	0.5	0.4	0.5	0.5	1.61774	2.39031	2.95552	2.39031
					1.0	1.59747	2.37679	2.67955	4.05128
					1.5	1.58143	2.36462	2.5756	3.94069
					2.0	1.57147	2.35697	2.5215	3.88348

Table 5. Nusselt number for higher values Re_r, Pr, B_1 and β.

Re_r	M	Q_1	B_1	Q_2	β	Pr	Nu_{ra} Fe_3O_4	Nu_{ra} Aggregation	Nu_{rb} Fe_3O_4	Nu_{rb} Aggregation
0.3	1.0	0.5	0.4	0.5	1.0	6.2	0.901395	0.903215	0.437520	0.457395
0.6							0.900171	0.905945	0.422796	0.454138
0.9							0.899351	0.905886	0.414839	0.449039
1.2							0.899074	0.905724	0.410834	0.445677
0.3	0.0	0.5	0.5	0.5	1.0	6.2	0.883823	0.888842	0.485561	0.502841
	0.5						0.891532	0.895359	0.459554	0.478391
	1.0						0.901397	0.903215	0.437521	0.457395
	1.5						0.909188	0.909387	0.414029	0.436354
0.3	1.0	0.3	0.5	0.5	1.0	6.2	0.901360	0.903183	0.437461	0.457335
		0.6					0.901415	0.903232	0.437550	0.457426
		0.9					0.901468	0.903280	0.437639	0.457517
		1.2					0.901522	0.903329	0.437727	0.457608
0.3	1.0	0.5	0.2	0.5	1.0	6.2	0.901395	0.903215	0.437520	0.457395
			0.6				0.901397	0.903215	0.437521	0.457395
			1.0				0.901397	0.903215	0.437521	0.457395
			1.4				0.901397	0.903215	0.437521	0.457395
0.3	1.0	0.5	0.5	0.2	1.0	6.2	0.900753	0.902628	0.435430	0.455262
				0.6			0.901619	0.903419	0.438228	0.458117
				1.0			0.902546	0.904273	0.441115	0.461060
				1.4			0.903540	0.905194	0.444094	0.464094
0.3	1.0	0.5	0.5	0.5	0.0	6.2	0.678303	0.903215	1.176870	0.457395
					0.5		0.974260	0.973073	0.451158	0.485320
					1.0		0.901397	0.903215	0.437521	0.457395
					1.5		0.860176	0.863914	0.413998	0.431130
0.3	1.0	0.5	0.5	0.5	1.0	6.2	0.901395	0.903215	0.437520	0.457395
						7.2	0.901734	0.903532	0.437180	0.457096
						8.2	0.902000	0.90378	0.436934	0.456875
						9.2	0.902214	0.90398	0.436749	0.456707

7. Concluding Remarks

In this article, the heat transfer analysis led to a discovery for Ferro Fe_3O_4 based nanofluids between two parallel rotating disks with pours medium. The aggregation nanoparticle, relaxation time, two kinds of heat sources (such as temperature and space-dependent heat source) are presented. The governing partial differential equation (PDEs) model is transformed into a nonlinear ordinary differential equations (ODEs) system by similarity transformation. The solution is computed for the transformed ODEs system by using a shooting scheme with the RK method. The velocity and temperature of the fluid are determined and presented. The physical quantities namely skin friction and Nusselt number are presented. The concluding remarks of this work are as follows

- The radial and axial velocity of the fluid reduces by higher-values $ß_1$ and $ß_2$ for Ferro Fe_3O_4 and Aggregation nanoparticle base fluid.

- The radial and axial velocity of the fluid reduces by higher-values ß$_1$ and ß$_2$ for Ferro Fe_3O_4 and Aggregation nanoparticle) based nanofliuid.
- A decline in the tangential velocity of nanofluid was noticed for magnetic parameter M, porous permeability parameter λ_1 and Reynolds number Re_r. Declines in the temperature of fluid for both (Ferro Fe_3O_4 and Aggregation nanoparticle) with parameters Pr, M, Ec, β and Re_r.
- There are increases in temperature of the fluid by greater values of B_1 for Ferro Fe_3O_4 and Aggregation nanoparticle base fluids.

Author Contributions: Funding acquisition, M.E. and M.Y.M.; Investigation, H.Z.; Supervision, H.A.W. and U.K. All authors have read and agreed to the published version of the manuscript.

Funding: The authors extend their appreciation to the Deanship of Scientific Research at King Khalid University for funding this work through Large Groups Project under grant number RGP–2-110/1443.

Institutional Review Board Statement: Not applicable.

Informed Consent Statement: Not applicable.

Data Availability Statement: Not applicable.

Conflicts of Interest: The authors declare no conflict of interest.

Nomenclature

Symbles	**Name**
MHD	Magnetohydrodynamics
IVP	Initial Value Problem
Ω_1 and Ω_2	Stretching rate constants
u, v, w	Velocity components
K_1, K_2	Velocity rate slip
M	Magnetic field parameter)
T_1, T_2	Temperature at lower and upper disc
Pr	Prandtl number
Cf_1 and Cf_2	Local skin friction at (lower disk and upper disk)
τ_w	total shear stress
ρ_{cp}	Specific heat at constant pressure
q_w	Wall heat flux
$Nu_x 1$	Nusselt number
D	Fractal index
k_a	Aggregate thermal conductivity
Re_r	Reynolds number
r_p and r_a	Nanoparticles and Radii of aggregates (m)
Q_1, Q_2	Heat sources
λ_2	Thermal relaxation
ß$_1$, ß$_2$, ß$_3$	Rotation parameters
RK	Runge-Kutta
BVP	Boundary value problem
r, θ and z	Cylindrical coordinates
$\hat{T}$	Temperature
P	Pressure
q	Heat flux
$\frac{r_a}{r_p}$	Diffusion-limited aggregation
$\mu_{nf}(\hat{T})$	Dynomic viscosity
γ_1, γ_2	Slip boundary conditions
τ_{rz} and $\tau_{\theta z}$	shear stress and tangential stress
f	Dimensionless velocity
ρ_{nf}	Density of the nanofluid,
c	Stretching rate constant
Υ	Thermal relaxation

ν	Kinematic viscosity
B_1, B_2	Biot numbers
ϕ_m	Maximum volume fraction of nanoparticles
η_a	Einstein coefficient
λ_1	Porosity parameter

References

1. Khanafer, K.; Vafai, K.; Lightstone, M. Buoyancy-driven heat transfer enhancement in a two-dimensional enclosure utilizing nanofluids. *Int. J. Heat Mass Transf.* **2003**, *46*, 3639–3653. [CrossRef]
2. Rostami, A.K.; Hosseinzadeh, K.; Ganji, D.D. Hydrothermal analysis of ethylene glycol nanofluid in a porous enclosure with complex snowflake shaped inner wall. *Waves Random Complex Media* **2020**, *32*, 1–18. [CrossRef]
3. Waini, I.; Ishak, A.; Pop, I. MHD flow and heat transfer of a hybrid nanofluid past a permeable stretching/shrinking wedge. *Appl. Math. Mech.* **2020**, *41*, 507–520. [CrossRef]
4. Devi, S.S.U.; Devi, S.A. Numerical investigation of three-dimensional hybrid Cu–Al_2O_3/water nanofluid flow over a stretching sheet with effecting Lorentz force subject to Newtonian heating. *Can. J. Phys.* **2016**, *94*, 490–496. [CrossRef]
5. Hosseinzadeh, K.; Roghani, S.; Asadi, A.; Mogharrebi, A.; Ganji, D.D. Investigation of micropolar hybrid ferrofluid flow over a vertical plate by considering various base fluid and nanoparticle shape factor. *Int. J. Numer. Methods Heat Fluid Flow* **2020**, *190*, 112–120. [CrossRef]
6. Shoaib, M.; Raja, M.A.Z.; Sabir, M.T.; Awais, M.; Islam, S.; Shah, Z.; Kumam, P. Numerical analysis of 3-D MHD hybrid nanofluid over a rotational disk in presence of thermal radiation with Joule heating and viscous dissipation effects using Lobatto IIIA technique. *Alex. Eng. J.* **2021**, *60*, 3605–3619. [CrossRef]
7. Hassan, M.; Marin, M.; Ellahi, R.; Alamri, S.Z. Exploration of convective heat transfer and flow characteristics synthesis by Cu–Ag/water hybrid-nanofluids. *Heat Transf. Res.* **2018**, *49*, 125394608. [CrossRef]
8. Dinarvand, S. Nodal/saddle stagnation-point boundary layer flow of CuO–Ag/water hybrid nanofluid: A novel hybridity model. *Microsyst. Technol.* **2019**, *25*, 2609–2623. [CrossRef]
9. Anuar, N.S.; Bachok, N.; Arifin, N.M.; Rosali, H. Effect of suction/injection on stagnation point flow of hybrid nanofluid over an exponentially shrinking sheet with stability analysis. *CDF Lett.* **2019**, *11*, 21–33.
10. Ahmed, A.; Nadeem, S. Effects of magnetohydrodynamics and hybrid nanoparticles on a micropolar fluid with 6-types of stenosis. *Results Phys.* **2017**, *7*, 4130–4139. [CrossRef]
11. Yousefi, M.; Dinarvand, S.; Yazdi, M.E.; Pop, I. Stagnation-point flow of an aqueous titania-copper hybrid nanofluid toward a wavy cylinder. *Int. J. Numer. Methods Heat Fluid Flow* **2018**, *28*, 1716–1735. [CrossRef]
12. Emslie, A.G.; Bonner, F.T.; Peck, L.G. Flow of a viscous liquid on a rotating disk. *J. Appl. Phys.* **1958**, *29*, 858–862. [CrossRef]
13. Rout, B.C.; Mishra, S.R.; Nayak, B. Semi-analytical solution of axisymmetric flows of Cu- and Ag-water nanofluids between two rotating disks. *Heat Transf.-Asian Res.* **2019**, *48*, 957–981. [CrossRef]
14. Khan, J.A.; Mustafa, M.; Hayat, T.; Turkyilmazoglu, M.; Alsaedi, A. Numerical study of nanofluid flow and heat transfer over a rotating disk using Buongiorno's model. *Int. J. Numer. Methods Heat Fluid Flow* **2017**, *48*, 221–234. [CrossRef]
15. Hayat, T.; Qayyum, S.; Imtiaz, M.; Alsaedi, A. Flow between two stretchable rotating disks with Cattaneo-Cristov heat flux model. *Result. Phys* **2017**, *48*, 126–133. [CrossRef]
16. Li, J.J.; Xu, H.; Raees, A.; Zhao, Q.K. Unsteady mixed bioconvection flow of a nanofluid between two contracting or expanding rotating discs. *Z. Naturforsch.* **2016**, *48*, 221–234. [CrossRef]
17. He, Y.; Jin, Y.; Chen, H.; Ding, Y.; Cang, D.; Lu, H. Heat transfer and flow behaviour of aqueous suspensions of TiO_2 nanoparticles (nanofluids) flowing upward through a vertical pipe. *Int. J. Heat Mass Transf.* **2007**, *50*, 2272–2281. [CrossRef]
18. Mackolil, J.; Mahanthesh, B. Inclined magnetic field and nanoparticle aggregation effects on thermal Marangoni convection in nanoliquid: A sensitivity analysis. *Chin. J. Phys.* **2020**, *69*, 24–37. [CrossRef]
19. Chen, J.; Zhao, C.; Wang, B. Effect of nanoparticle aggregation on the thermal radiation properties of nanofluids: An experimental and theoretical study. *Int. J. Heat Mass Transf.* **2020**, *154*, 119690. [CrossRef]
20. Wang, F.; Rani, S.P.; Sarada, K.; Gowda, R.P.; Zahran, H.Y.; Mahmoud, E.E. The effects of nanoparticle aggregation and radiation on the flow of nanofluid between the gap of a disk and cone. *Case Stud. Therm. Eng.* **2022**, *33*, 101930. [CrossRef]
21. Wang, F.; Kumar, R.N.; Prasannakumara, B.C.; Khan, U.; Zaib, A.; Abdel-Aty, A.H.; Yahia, I.S.; Alqahtani, M.S.; Galal, A.M. Aspects of Uniform Horizontal Magnetic Field and Nanoparticle Aggregation in the Flow of Nanofluid with Melting Heat Transfer. *Nanomaterials* **2022**, *12*, 1000. [CrossRef]
22. Aziz, A.; Jamshed, W.; Aziz, T.; Bahaidarah, H.; Ur Rehman, K. Entropy analysis of Powell–Eyring hybrid nanofluid including effect of linear thermal radiation and viscous dissipation. *J. Therm. Anal. Calorim.* **2021**, *143*, 1331–1343. [CrossRef]
23. Saif, R.S.; Muhammad, T.; Sadia, H.; Ellahi, R. Boundary layer flow due to a nonlinear stretching curved surface with convective boundary condition and homogeneous and heterogeneous reactions. *Phys. A* **2020**, *551*, 123996. [CrossRef]
24. Hayat, T.; Saif, R.S.; Ellahi, R.; Muhammad, T.; Ahmad, B. Numerical study of boundary-layer flow due to a nonlinear curved stretching sheet with convective heat and mass conditions. *Result Phys.* **2017**, *7*, 2601–2606. [CrossRef]
25. Saleem, S.; Nadeem, S.; Rashidi, M.M.; Raju, C.S.K. An optimal analysis of radiated nanomaterial flow with viscous dissipation and heat source. *Microsyst. Technol.* **2019**, *25*, 683–689. [CrossRef]

26. Zia, Q.Z.; Ullah, I.; Waqas, M.A.; Alsaedi, A.; Hayat, T. Cross diffusion and exponential space dependent heat source impacts in radiated three-dimensional (3D) flow of Casson fluid by heated surface. *Results Phys.* **2018**, *8*, 1275–1282.
27. Mahanthesh, B.; Mackolil, J.; Shehzad, S.A. Statistical analysis of stagnation-point heat flow in Williamson fluid with viscous dissipation and exponential heat source effects. *Heat Transf.* **2020**, *49*, 4580–4591. [CrossRef]
28. Gireesha, B.; Kumar, P.S.; Mahanthesh, B.; Shehzad, S.; Abbasi, F. Nonlinear gravitational and radiation aspects in nanoliquid with exponential space dependent heat source and variable viscosity. *Microgravity Sci. Technol.* **2018**, *30*, 257–264. [CrossRef]
29. Hayat, T.; Waqas, M.; Khan, M.I.; Alsaedi, A.; Shehzad, S. Magnetohydrodynamic flow of burgers fluid with heat source and power law heat flux. *Chin. J. Phys.* **2017**, *55*, 318–330. [CrossRef]
30. Said, Z.; Sharma, P.; Sundar, L.S.; Afzal, A.; Li, C. Synthesis, stability, thermophysical properties and AI approach for predictive modelling of Fe_3O_4 coated MWCNT hybrid nanofluids. *J. Mol. Liq.* **2021**, *340*, 117291. [CrossRef]
31. Said, Z.; Sundar, L.S.; Tiwari, A.K.; Ali, H.M.; Sheikholeslami, M.; Bellos, E.; Babar, H. Recent advances on the fundamental physical phenomena behind stability, dynamic motion, thermophysical properties, heat transport, applications, and challenges of nanofluids. *Phys. Rep.* **2021**, *946*, 1–94. [CrossRef]
32. Negi, A.S.; Kumar, B.; Kumar, A.; Kumari, C.; Prachi, K.; Chamkha, A.J. Transportation of TiO_2/GO–H_2O hybrid nanofluid between two discs. *Indian J. Pysics* **2021**. [CrossRef]
33. Esfandiari, R.S. *Numerical Methods for Engineers and Scientists Using MATLAB*; CRC Press: Boca Raton, FL, USA, 2013.
34. Hosseinzadeh, K.; Asadi, A.; Mogharrebi, A.; Khalesi, J.; Mousavisani, S.; Ganji, D. Entropy generation analysis of $(CH_2OH)_2$ containing CNTs nanofluid flow under effect of MHD and thermal radiation. *Case Stud. Therm. Eng.* **2019**, *14*, 100482. [CrossRef]
35. Raju, S.S.K.; Babu, M.J.; Raju, C. Irreversibility analysis in hybrid nanofluid flow between two rotating disks with activation energy and cross-diffusion effects. *Chin. J. Phys.* **2021**, *72*, 499–529. [CrossRef]